Computer Methods and Programs in Biomedicine 242 (2023) 107834

Contents lists available at ScienceDirect

Computer Methods and Programs in Biomedicine

journal homepage: www.elsevier.com/locate/cmpb

# Physics-informed neural network for fast prediction of temperature distributions in cancerous breasts as a potential efficient portable AI-based diagnostic tool

Olzhas Mukhmetov [a], Yong Zhao [a], Aigerim Mashekova [a], Vasilios Zarikas [b,c], Eddie Yin Kwee Ng [d,*], Nurduman Aidossov [a]

[a] School of Engineering and Digital Sciences, Nazarbayev University, Astana 010000, Kazakhstan
[b] Department of Mathematics, University of Thessaly, Volos, Greece
[c] Mathematical Sciences Research Laboratory (MSRL), Lamia 35100, Greece
[d] School of Mechanical and Aerospace Engineering, Nanyang Technological University, Singapore 639798, Singapore

ARTICLE INFO

*Key words:*
Physics-informed neural network
Finite Element Analysis
Thermography
Breast cancer

ABSTRACT

This work presents the development of a novel Physics-Informed Neural Network (PINN) method for fast forward simulation of heat transfer through cancerous breast models. The proposed PINN method combines deep learning and physical principles to predict the temperature distributions in breast tissues and identify potential abnormal regions indicating the presence of tumors. The PINN model is normally trained by physics in terms of the residuals of the heat transfer equation, as well as boundary conditions with and without datasets of surface thermal imaging data concerning cancerous breast tissues, which can be used for future inverse thermal modeling to calculate tumor sizes and locations. The model is validated by comparing its predictions with those obtained by traditional Finite Element Analysis (FEA) for various cases. The comparison validates the PINN model as an accurate and fast method for thermal modeling and breast cancer diagnostic tool as the PINN simulation is found to be around 12 times faster than its FEM counterpart. The utilization of deep learning and physical principles in a diagnostic tool provides a non-invasive and safer alternative for breast self-examination compared to traditional methods such as mammography. These findings hold promise for the ongoing development of a new portable Artificial Intelligence (AI) tool for the early detection of breast cancer in breast self-examination as promoted by WHO, which is crucial for reducing mortality rates of breast cancer in the world.

## 1. Introduction

Globally, breast cancer is the most common cancer among women, with an estimated 2.1 million new cases and 627,000 deaths in 2020. According to the World Health Organization (WHO), the incidence of breast cancer is increasing in many low- and middle-income countries, likely due to increasing life expectancy and changes in lifestyle and reproductive patterns.

Early detection and diagnosis of breast cancer are crucial for improving patient outcomes and reducing mortality rates. One of the most effective methods for early detection is mammography, which can detect small tumors that may not be palpable during a physical examination [1–3]. In addition to mammography, ultrasound and Magnetic Resonance Imaging (MRI) can also be used to diagnose breast cancer in its early stages.

Furthermore, one of the important aspects of early diagnosis is Breast Self-Examination (BSE), which involves regularly checking the breasts for changes such as lumps or thickening of the tissue. BSE, along with Clinical Breast Examination (CBE) performed by a healthcare provider, can help to identify breast cancer in its early stages before it becomes palpable [1–3]. Taking into account recent development of technologies and particularly artificial intelligence (AI) they also can be used as BSE tool. In this regard the physics-informed neural network (PINN) algorithm based on heat transfer can simulate and identify abnormalities that may be missed by human interpretation [4].

One of the main advantages of thermal imaging and Neural Network (NN) are tools that can detect breast cancer in its early stages before it becomes palpable [5]. This is important because early detection is

* Corresponding author.
*E-mail address:* mykng@ntu.edu.sg (E.Y.K. Ng).

https://doi.org/10.1016/j.cmpb.2023.107834
Received 14 June 2023; Received in revised form 18 September 2023; Accepted 27 September 2023
Available online 29 September 2023

crucial for improving patient outcomes and reducing mortality rates [1–3]. Another advantage of thermal imaging and NN is that it is non-invasive and does not expose the patient to ionizing radiation, as in the case of mammography. This makes it a safer option for BSE, especially for women who are at a higher risk of developing breast cancer or have a family history of the disease [6].

## 2. Related works

Several studies have compared the performance of Finite Element Analysis (FEA) and PINN for solving partial differential equations (PDEs) in various applications, including heat transfer problems. Raissi et al. (2019) [7] studied the accuracy and computational efficiency of FEA and PINN for solving the Poisson equation in a square domain. They found that PINN outperformed FEA in terms of accuracy, while FEA was more computationally efficient for fine meshes. In other words, coarse mesh leads to the decrease of the accuracy of FEA, while PINN maintains its accuracy. Li et al. (2022) [8] studies showed that by integrating the governing heat conduction equations into the architecture of NNs, PINNs can effectively simulate and predict heat distribution within various systems. This approach allows PINNs to learn the underlying physics of heat transfer while adapting to complex geometries and boundary conditions. As a result, PINNs offer a versatile and efficient way to compute temperature profiles and thermal behaviors, making them valuable in fields ranging from engineering and materials science to environmental studies.

Zhili He et al. (2021) studied a novel data-driven approach utilizing Physical Information Neural Networks (PINNs) for analyzing and inverting parameters in heat conduction problems. It covers both direct analysis and parameter inversion concurrently, offering an adapted PINNs framework with flexible activation functions. Case studies involving wood and steel demonstrate the framework's satisfactory accuracy and its potential to replace finite element modeling in part. The inverse analysis focuses on inverting both constant and variable parameters, utilizing neural network frameworks with linked connections. Experimental results indicate accurate inversion of unknown parameters in the heat conduction equation with high computational efficiency. Compared to traditional methods, this framework offers a unified solution for both direct and inverse heat conduction problems, with wide applications in materials science.

The study of Shengze Cai et al. (2021) explores the application of Physics-Informed Neural Networks (PINNs) in addressing intricate heat transfer problems within engineering. PINNs prove to be highly effective in handling issues characterized by noisy data and incomplete physics. Various scenarios, including those involving unknown thermal boundary conditions and two-phase flow problems, are investigated. The findings underscore the capability of PINNs to tackle ill-posed problems and facilitate the integration of computational and experimental heat transfer research, extending to practical industrial applications.

This paper presents the development of a PINN code for the forward simulation of heat transfer inside a breast with a tumor. The hypothesis is whether the developed PINN code will be able to accurately predict the temperature distribution around a tumor on the breast by solving a partial differential equation of heat transfer.

The PINN code combines deep learning and physical principles to simulate the temperature distribution in the breast tissue and identify potential abnormal regions that may indicate the presence of a tumor. Furthermore, the PINN code will be trained by using a database of thermal images and compared with the temperature distribution obtained from FEA. The comparison will evaluate the accuracy and reliability of the PINN code, demonstrating its potential as a novel and innovative approach to medical imaging and cancer diagnosis.

## 3. Methodology

### A Governing Partial Differential Equation (PDE)

The equation of heat transfer is embedded into the PINN code, used for FEA, and formulated as follows:

$$\rho c\frac{\partial T}{\partial t} = k\frac{\partial^2 T}{\partial x^2} + k\frac{\partial^2 T}{\partial y^2} + k\frac{\partial^2 T}{\partial z^2} + Q \tag{1}$$

where, $c$ is the specific heat for unit mass, ρ is the density, Q is the rate of heat generation of the tissue, and k is the thermal conductivities.

The neural network prediction aims to solve the one-dimensional heat equation for any boundary conditions without heat transfer. The heat transfer partial differential equation (PDE) residual at any point can be assessed through the:

$$Error_{PDE} = \frac{k}{\rho c}\frac{\partial^2 T(x,t)}{\partial x^2} - \frac{\partial^2 T(x,t)}{\partial t} \tag{2}$$

If the neural network has received the proper training and its prediction accurately solves the one-dimensional heat equation, the error term will be close to zero at all points. Dirichlet boundary condition specifies the temperature of the surface at a given location. It states that the temperature at a particular point on the boundary is known and constant. The equation for the Dirichlet boundary condition is given by:

$$T(x,y,t) = T_0(x,y) \tag{3}$$

where $T_0$ $(x, y)$ is the specified temperature at the boundary and (x, y) is the location on the boundary.

Neumann boundary condition specifies the heat flux, or the rate of heat transfer through the surface, at a given location. It states that the normal derivative of the temperature at a particular point on the boundary is known. The equation for the Neumann boundary condition is given by:

$$k\frac{\partial T}{\partial n}|_B = h[T_B - T_\infty] \tag{4}$$

where $q_0$ $(x, y)$ is the specified heat flux at the boundary and $(x, y)$ is the location on the boundary. The symbol $\partial T/\partial n$ represents the normal derivative of the temperature and represents the rate of heat transfer through the surface in the direction normal to it.

It is essential to establish an initial condition, to successfully solve the transient heat conduction equation. This initial condition should clearly define the temperature distribution within the solid at the commencement of the time frame under consideration.

$$T(x,t_0) = \underline{T}(x,t) \tag{5}$$

where, $\underline{T}(x,t)$ is the initial temperature distribution.

### B The architecture of the Physics-Informed Neural Network

The architecture of PINN consists of an input layer that accepts the initial temperature distribution, 5 hidden layers that perform linear summation and non-linear transformations on the input layer, and finally an output layer that predicts the temperature distribution at a later time. The training process consisted of forward pass and backpropagation. In backpropagation a loss function (or cost function) measured the difference between the predicted and actual temperatures, and can be described as:

$$L_{Re} = \sum_{i=1}^{N}\left|\rho c\frac{\partial T_i}{\partial t} - k\nabla^2 T_i - q_v\right| \tag{6}$$

$$L_{IC} = \sum_{i=1}^{N}\left|T_{x,y,t_0} - T_i\right| \tag{7}$$

$$L_{BC} = \sum_{i=1}^{N}|T_B - T_i| + \sum_{i=1}^{N}\left|k\frac{\partial \mathrm{T_i}}{\partial n} - h(T_i - T_\infty)\right| \tag{8}$$

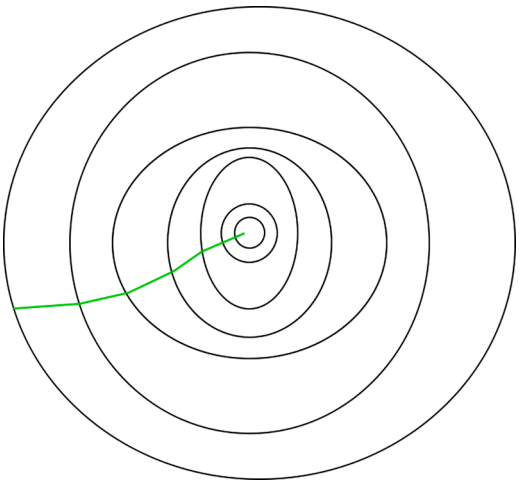

**Fig. 1.** Path of gradient descent method to minimum.

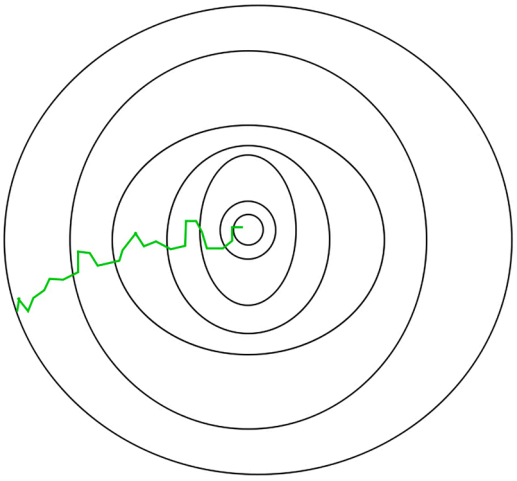

**Fig. 2.** Path of stochastic gradient descent method to minimum.

$$Loss = L_{Re} + L_{IC} + L_{BC} \tag{9}$$

where $L_{Re}$ – residual loss, $L_{IC}$ – initial condition, $L_{BC}$ – boundary condition.

During the backpropagation, an optimization algorithm was explored to update the network parameters by computing the gradient of the loss function training process, to minimize the loss function, improve accuracy and evaluation process, and to assess the performance of the trained model on a validation.

PINNs typically have a specific structure of layers that correspond to the input, output, and hidden layers of traditional neural networks, but also include physics-informed layers that capture the PDEs. The training process of PINNs involves solving a system of equations that combines the PDEs with data-driven neural network approximations. This is accomplished by optimizing the neural network parameters to minimize the loss function, consisting of residuals of the discrete PDEs at a set of collocation points in the domain, the boundary conditions and the errors between the input data and the neural network predictions if any. The optimization process is performed using stochastic gradient descent method, which iteratively updates the neural network parameters to minimize the loss function.

Gradient descent and stochastic gradient descent are two optimization algorithms that are commonly used to train deep neural networks. Gradient descent works by iteratively updating the parameters of a model in the direction of the negative gradient of the loss function. Stochastic gradient descent is a variation of gradient descent that updates the parameters at stochastically selected collocation points in the domain. This can be more efficient than gradient descent, but it can also be less accurate. Mini-batch gradient descent is a further variation of stochastic gradient descent that updates the parameters after a small batch of training examples. This can be a good compromise between the efficiency of stochastic gradient descent and the accuracy of gradient descent.

The goal of optimization is to find the best possible set of parameters for a model. This is done by minimizing a loss function, which measures how well the model fits the data. The gradient descent algorithm is a method for finding the best parameters by iteratively updating the parameters in the direction of the steepest loss gradient:

$$\theta_{n+1} = \theta_n - \alpha \cdot \nabla L(\theta_n) \tag{7}$$

where $\alpha$ is the learning rate. Stochastic gradient descent (SGD) is a variation of gradient descent that uses a stochastically selected mini-batch of data to calculate the gradient of the loss function. This can be more efficient than using the entire dataset.

The path taken by batch gradient descent is a smooth, continuous line that moves towards the minimum of the loss function (Fig. 1).

The path taken by SGD is often more erratic than the path taken by batch gradient descent (Fig. 2).

Although SGD requires a greater number of iterations to attain the minimum than traditional Gradient Descent, it is computationally significantly less expensive. As a result, SGD is recommended over Batch Gradient Descent for improving a learning algorithm in most cases.

### C Neural network

The PINN method was utilized to model heat transfer through cancerous breast tissue [9–13]. The model used in this study is a fully connected neural network, and the Adam optimizer was employed to ensure the accuracy and efficiency of the model. This optimization algorithm utilizes the first and second moments of the gradient to update the model's parameters dynamically. The algorithm adjusts the learning rate based on the gradient direction and magnitude, facilitating faster convergence and avoiding local minima or saddle points [14]. The use of the Adam optimizer in this study enabled more efficient and accurate training of the model. Additionally, the tanh activation function was utilized in the neural network. This function maps inputs to a range between −1 and 1, which is particularly useful for modeling data with both positive and negative values. Moreover, the tanh function is differentiable, facilitating efficient gradient computation during back-propagation and optimization [15]. The use of the tanh activation function enabled the model to capture non-linear relationships between input and output variables more accurately [16–19].

The architecture was defined using a list called layer_size, which contained the number of nodes in each layer of the neural network.

The list layer_size array was initialized with a total of 7 elements. The first element, which represented the number of input features, was set to 4. The subsequent 5 elements were set to 60, which represented the number of neurons in each of the 5 hidden layers of the neural network. The final element of the list was set to 1, representing the number of output nodes in the neural network. Therefore, the total number of neurons in this neural network architecture is 301 (Fig. 3).

### D Optimization method

The optimization was based on the LBFGS (Limited-memory Broyden-Fletcher-Goldfarb-Shanno) method. L-BFGS is a popular optimization algorithm used to solve unconstrained optimization problems. It is a quasi-Newton method that uses a limited amount of memory to approximate the Hessian matrix of the objective function.

The L-BFGS algorithm works by iteratively updating the solution

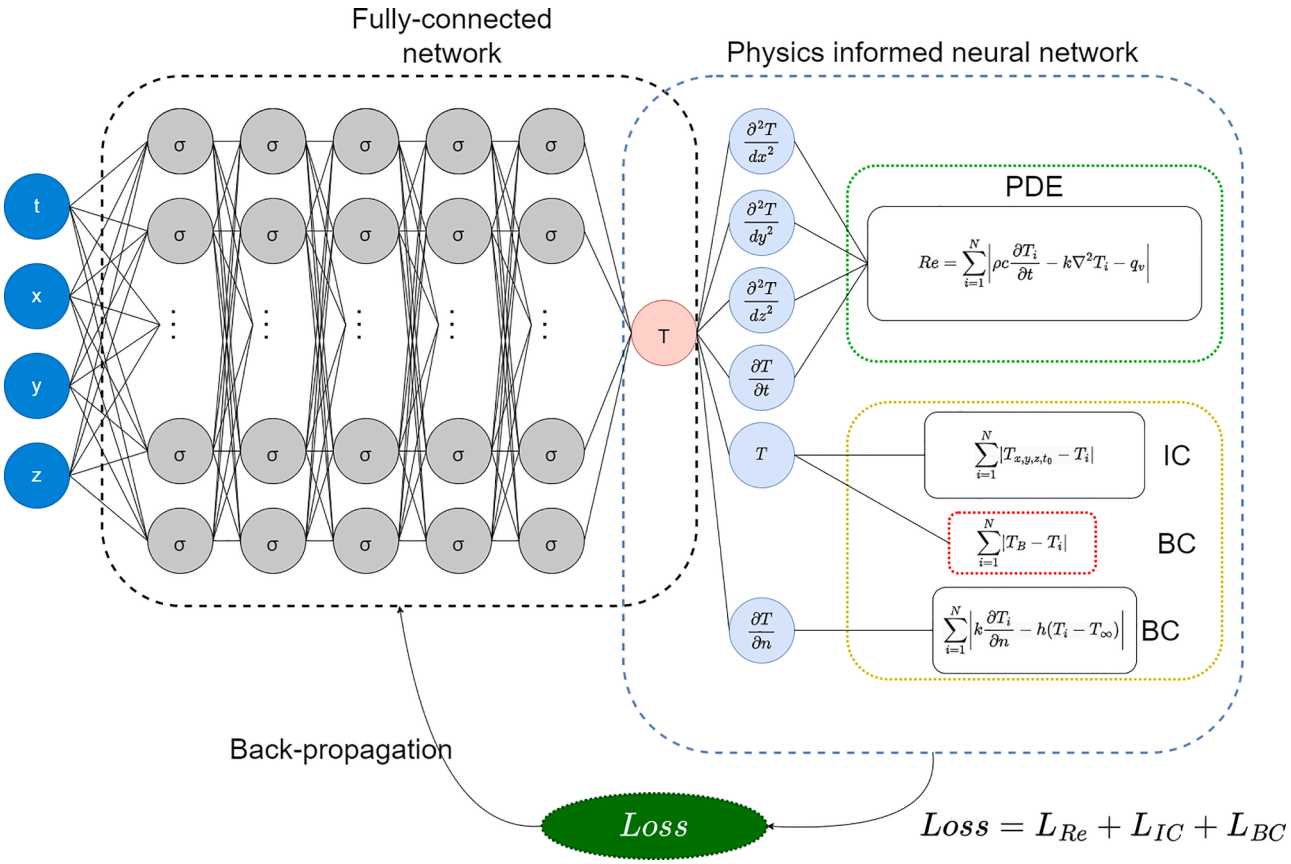


**Fig. 3.** The architecture of PINN for heat transfer through a solid body.

using the gradient information of the objective function. At each iteration, the algorithm uses a stored history of past gradients and solution updates to construct an approximate Hessian matrix. The inverse of this approximate Hessian matrix is then used to find the next solution update, which is taken in the direction that reduces the objective function the most.

Let's have the function $f(x, y)$ be given and we solve an optimization problem: min $f(x, y)$. Here in the general case $f(x, y)$ is a non-convex function which has continuous second derivatives. The following is the algorithm:

1) Initialize starting point $x_0$
2) Set the search accuracy
3) Define the initial approximation $H_0 = B_0^{-1}$, where $B_0^{-1}$ is the inverse hessian of the function
4) Find the point in the direction of the search, which is defined as follows:

$$p_k = -H_k * \nabla f_k$$

5) Calculate $x_{k+1}$ through a recurrence relation:

$$x_{k+1} = x_k + k * p_k$$

6) The coefficient $k$ is found using a line search, where $k$ satisfies Wolfe's conditions

$$f(x_k + k * p_k) \le f(x_k) + c_1 * k * \nabla f_k^T * p_k$$

$$\nabla f(x_k + k * p_k)^T * p_k \ge c_2 * \nabla f_k^T * p_k$$

7) Define the vectors:

$$s_k = x_{k+1} - x_k$$

$$y_k = \nabla f_{k+1} - \nabla f_k$$

$s_k$ is the step of the algorithm per iteration, $y_k$ is the gradient change per iteration.

8) Update the hessian function according to the following formula:

$$H_{k+1} = \left(I - k * s_k * y_k^T\right) H_k \left(I - k * y_k * s_k^T\right) + * s_k * s_k^T$$

where $k$

$$k = \frac{1}{y_k^T s_k}$$

The algorithm continues as long as the inequality is true: $|\nabla f_k| > \epsilon$.

L-BFGS is memory-efficient thanks to its limited-memory approach, making it suitable for optimization problems with modern numbers of variables. It performs well for problems with moderate dimensions, making it a practical choice for various optimization tasks. L-BFGS exhibits fast convergence, especially when the initial guess is close to a local minimum, allowing for efficient optimization in such scenarios [20].

Adam is well-suited for training deep neural networks with a large number of parameters, making it a popular choice in the field of deep learning. Its adaptive learning rate mechanisms enable efficient convergence by individually adjusting learning rates for each parameter,


**Fig. 4.** Equipment used for measurements: a) IRTIS 2000ME; b) Fluke TiS60+ c) 3D Scanner Sense 2.

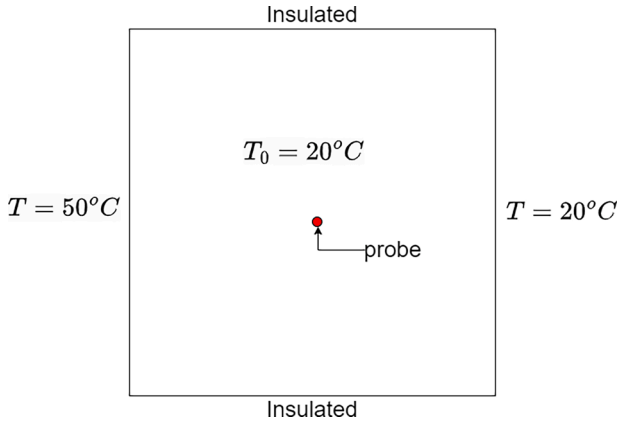


**Fig. 5.** Body diagram of the 2D model with boundary conditions.

**Table 1**
Heat parameters of human tissue.

| Tissue | Thermal conductivity (W/m-K) | Metabolic heat generation ($W/m^2$) |
|---|---|---|
| Gland | 0.48 | 800 |

improving optimization efficiency. Adam performs effectively in handling non-convex optimization problems, making it versatile for various optimization tasks, including those with complex objective functions [21].

## E Database

The study involves collecting patient data at the Multifunctional Medical Center of Astana city (Republic of Kazakhstan). The Medical center focuses on treating different oncology illnesses, including breast cancer. The study was approved by Nazarbayev University Institutional Research Ethics Committee (identification number is 592/21,072,022 from 21 July 2022).

Patient data includes thermograms and 3D breasts models, and other correlated factors that can influence the development of breast cancer. Thermograms show the temperature distribution on the surface of the breast, whereas 3D models of the breast present a specified breast model of each particular woman, which are used as input of the proposed method of tumor detection. The collected data are explored to generate 3D solid models, which were manipulated and processed in the CAD system and then used for Finite Element Analysis and PINN models.

Thermograms were collected using IR camera IRTIS 2000ME and Fluke TiS60+ (Fig. 4a, b) which are used for medical research and in the diagnosis of a wide range of illnesses, including oncological diseases.

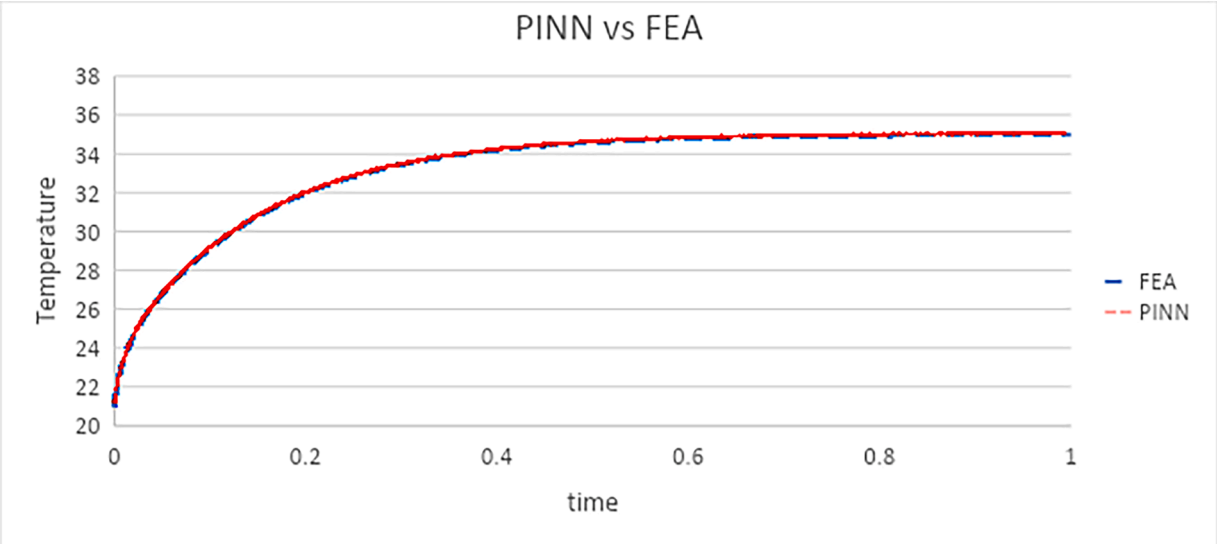


**Fig. 6.** PINN vs FEA temperature at the center point.

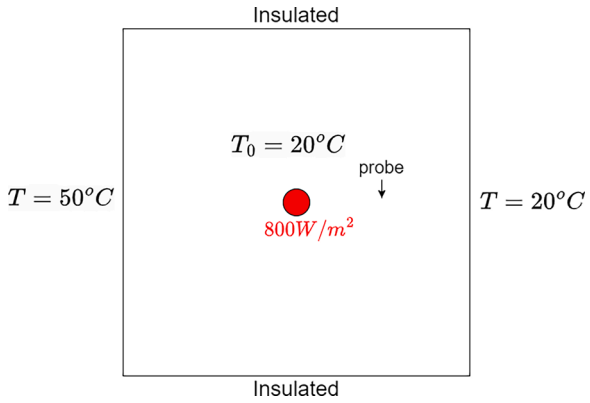


**Fig. 7.** Body diagram of the 2D model with heat generation.

The temperature resolution of IRTIS 2000ME for the entire field of view is 0.02 °C and temperature measurement accuracy is 0.1 °C. Accuracy of the Fluke IR camera is ±2 °C or 2%. 3D models were collected using a 3D Scanner called Sense 2 from 3D Systems which is a very light and easy-to-use scanner with excellent resolution, used for scanning objects from 200 to 2000 mm, and with a scanning accuracy of 0.9 mm (Fig. 4c).

In this research two key tools were used: Spyder, an integrated development environment (IDE) tailored for scientific computing and data analysis, and the Deepxde library, specializing in solving partial differential equations (PDEs) and inverse problems using deep learning techniques. Spyder's features, including code editing, interactive consoles, and data visualization, have streamlined my research workflow. On the other hand, Deepxde has enabled efficient PDE solving, handling of inverse problems, customizable neural network architectures, scalability, and integration with other deep learning libraries. Simulations were conducted on a high performance computer with Intel Xeon Silver 4210 processor, which has 10 cores and 20 threads, RAM of 64 GB.

Ansys transient thermal model was used as a FEA solver. This solver is designed to take advantage of parallel processing and multi-core

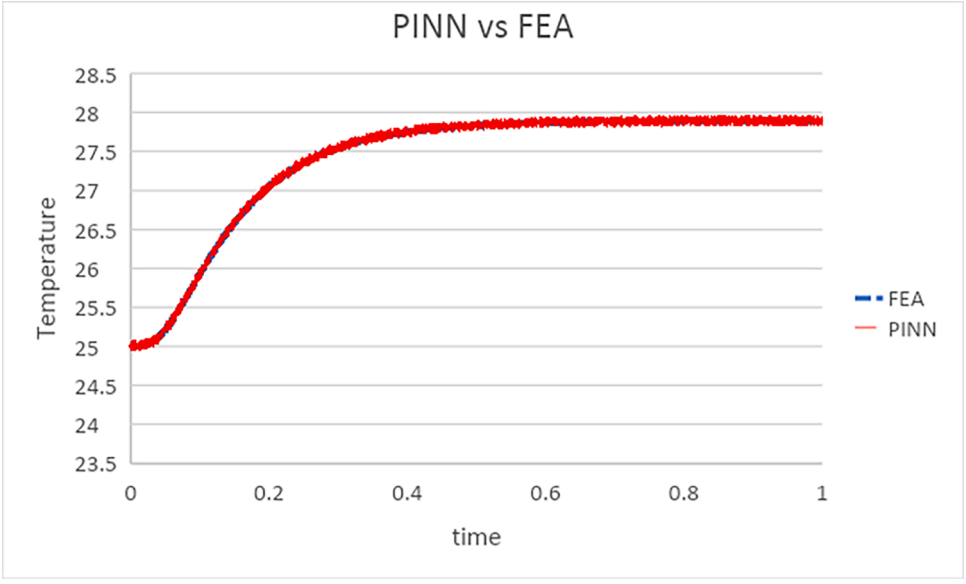


**Fig. 8.** PINN vs FEA temperature at the probe (with heat generation model).

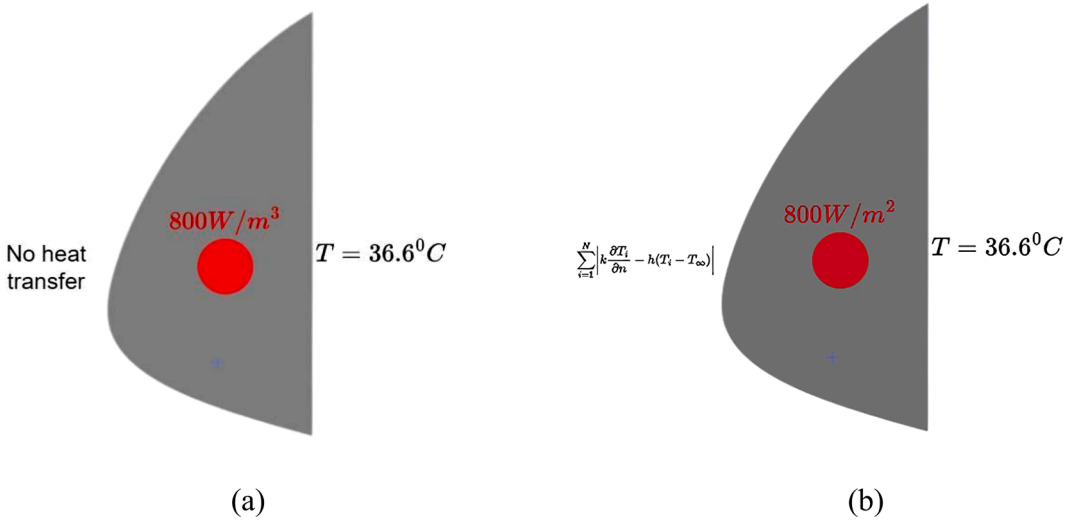


**Fig. 9.** Cross-sectional view 3D breast models with heat generation: *a*) adiabatic surface condition; *b*) convection heat transfer surface condition.

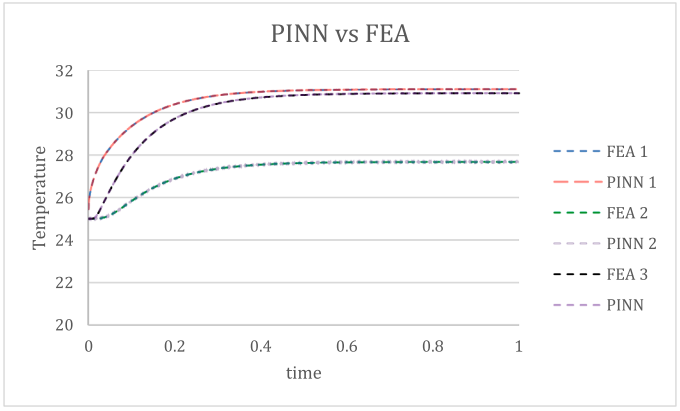


**Fig. 10.** PINN vs FEA temperature at the 3 probes for case (*a*).

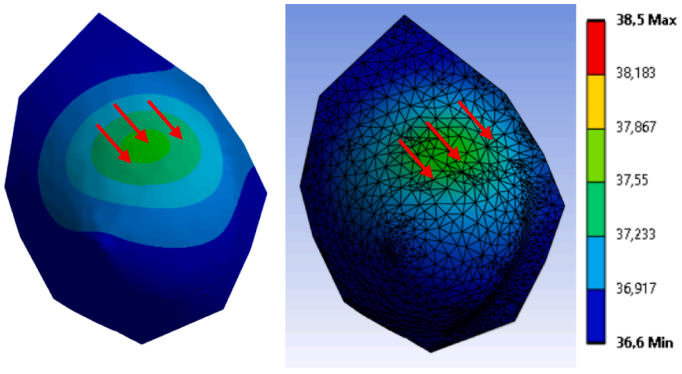


**Fig. 11.** PINN vs FEA temperature contour ($t = 0$) for case (*a*).

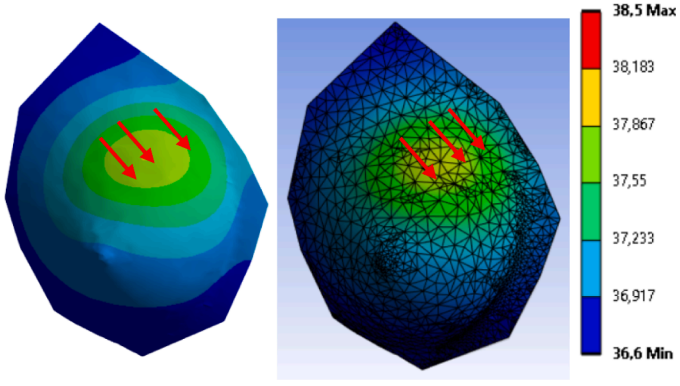


**Fig. 12.** PINN vs FEA temperature contour ($t = 0.5$) for case (*a*).

CPUs, enabling faster solution times for large and complex simulations. at involve changes over time, such as dynamic structural analysis or transient thermal analysis.

## 4. Results and discussion

### B 2D body validation

The PINN's efficacy was thoroughly evaluated by comparing its predictions with those obtained through a FEA. The objective of training the PINN was to predict the time-dependent solution of the two-dimensional heat equation in a body with a 1 m thickness, utilizing a uniform initial temperature boundary condition $T = 20$ °C. The constant temperature on one side is 20 °C and on another side is 50 °C, top and bottom walls insulated (Fig. 5). Table 1 shows thermal conductivity and metabolic heat generation of human body tissue [17].

A finite element simulation of an identical problem was run to validate the PINN predictions. As it can be seen from Fig. 6, PINN's

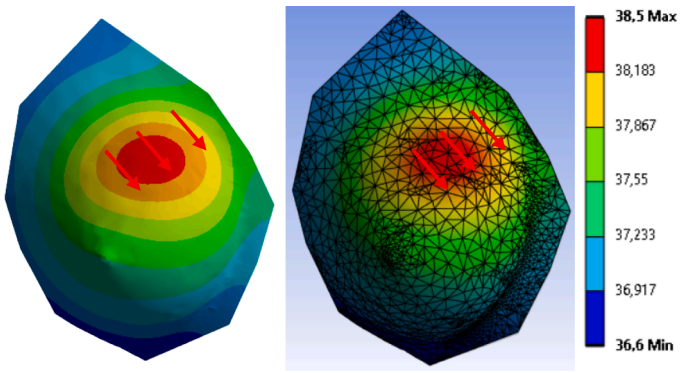


**Fig. 13.** PINN vs FEA temperature contour ($t = 1$) for case ($a$).

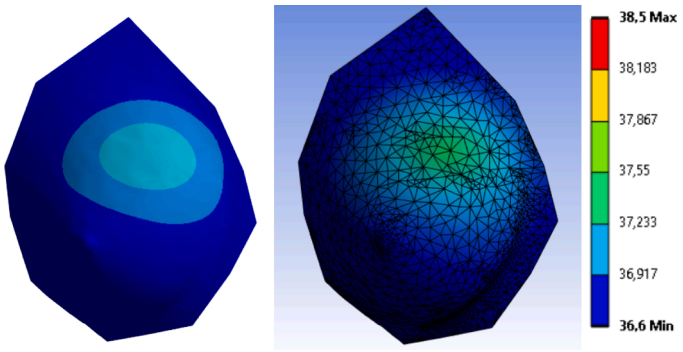


**Fig. 14.** PINN vs FEA temperature contour ($t = 0$) for case ($b$).

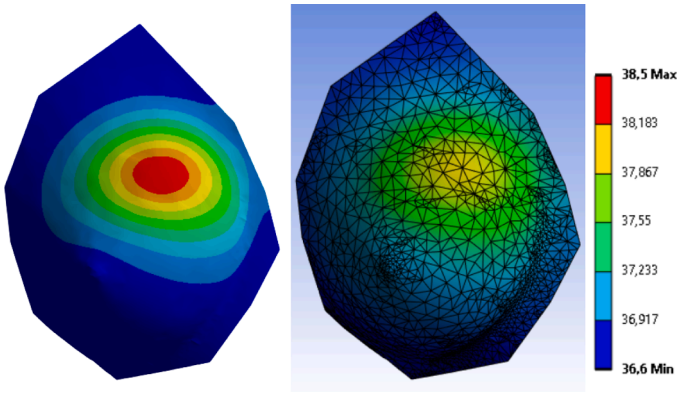


**Fig. 15.** PINN vs FEA temperature contour ($t = 0.5$) for case ($b$).

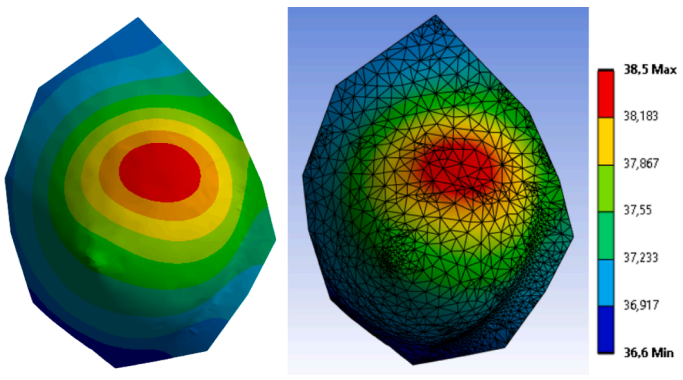


**Fig. 16.** PINN vs FEA temperature contour ($t = 1$) for case ($b$).

**Table 2**
Validation of PINN by FEA.

| Time | Temperature PINN [°C] | Temperature FEA [°C] | Accuracy [%] |
|---|---|---|---|
| 0.5 | 36.9 | 37.21 | 0.83 |
| 1 | 38.52 | 38.65 | 0.34 |

**Table 3**
Temperature difference between PINN and FEA.

| Time | Temperature PINN [°C] | Temperature FEA [°C] | Difference [%] |
|---|---|---|---|
| 0.5 | 38.3 | 38.2 | 0.26 |
| 1 | 38.45 | 38.56 | 0.29 |

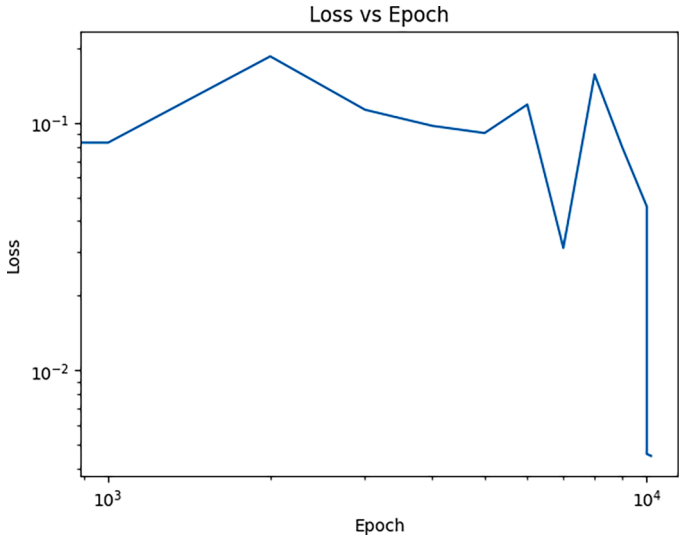


**Fig. 17.** Loss vs epoch.

predictions have been validated for a time-dependent solution of the two-dimensional heat equation in a body with a 1 m thickness, utilizing a uniform initial temperature boundary condition $T = 20$ °C.

### A 2D model validation with heat generation

The 2D model with a size of 1 meter was used to simulate heat transfer with the hot spot. The constant temperature on one side was 20 °C, and on the other side was set to 50 °C. Right on the center hot spot, which imitates tumor, with the heat generation of 800 W/m$^2$ was implemented (Fig. 7).

To validate the PINN model, the same model was set in the FEA program. The temperature at the probe was recorded and compared, so it can be seen as a good coincidence of two models, which allows us to use models for further simulation (Fig. 8).

### C 3D real breast model

To test the PINN tool on the simulation of heat transfer for the real cases 3D real breast model was used. Fig. 9 shows a cross-sectional view of a real breast geometric model with different surface conditions. The internal body temperature was set to 37 °, without heat loss on the skin surface in case ($a$) and convection heat loss with a heat transfer coefficient $h = 10$ W/(m$^2$C) in ($b$). Generalized physical parameters, such as density, thermal conductivity, and specific heat capacity, of human tissue were used [17,18].

To compare results from multiple probes in the same locations temperatures were computed. The temperature change from the time-

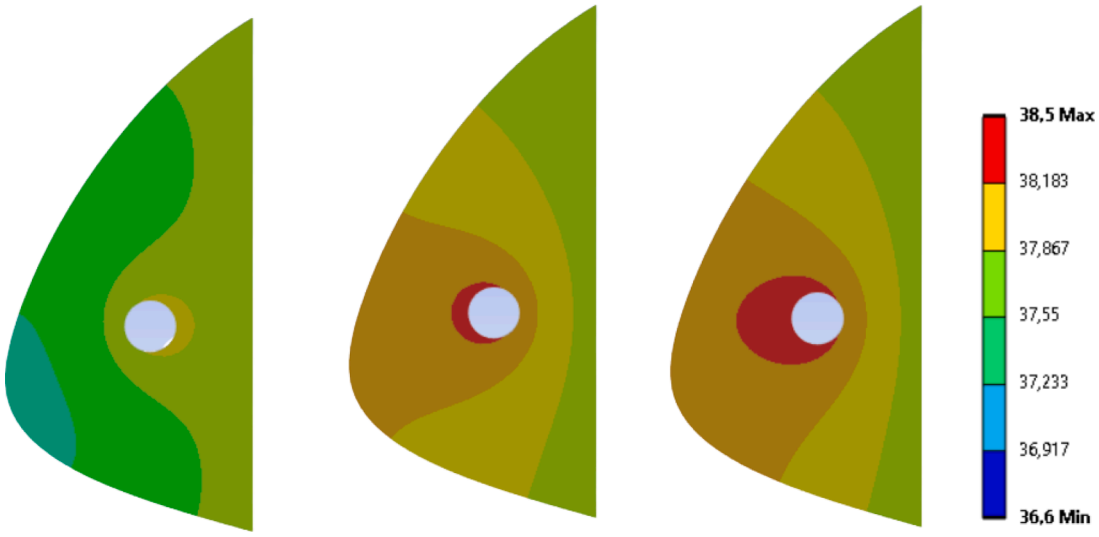


**Fig. 18.** PINN temperature contour ($t = 0$, $t = 0.5$, $t = 1$) for case ($b$).

**Table 4**
FEA vs PINN time spent for simulation.

| Tool | Total time [s] | Simulation time [s] |
|---|---|---|
| FEA | 229 | 229 |
| PINN | 288 | 20 |

dependent simulation for case ($a$) was compared in Figs. 10–16 (Table 2).

A 3D model of a real breast with heat loss on the skin surface was also used to evaluate the PINN tool's performance in calculating heat transfer in the breast model (Table 3, Fig. 17). To simulate the heat transfer mechanism, the simulation included generalized physical factors such as density, thermal conductivity, and specific heat capacity of human tissue (Fig. 18). In addition to these characteristics, the heat loss coefficient $h$ on the skin surface was set to an average value of 10 W/($m^2$·K) [16].

Finite element analysis for a 3D model of breast with heat convection took 3 min 49 s, while PINN was conducted in 4 min and 48 s. However, most of the time PINN spent for training, and simulation time is 20 s, which is almost 12 times faster than FEA (Table 4).

## 5. Conclusion

In conclusion, this paper presents a significant advancement in the field of breast cancer simulation and detection. The proposed physics-informed neural network (PINN) code leverages the power of deep learning and physical principles to simulate the temperature distribution in the breast tissue and identify potential abnormal regions that may indicate the presence of a tumor. The PINN code was trained by physics in terms of the residuals of the heat transfer equation, as well as boundary conditions with and without datasets of surface thermal imaging data concerning cancerous breast tissues, which can be used for future inverse thermal modeling to calculate tumor sizes and locations. The PINN model was compared with temperature distributions obtained from finite element analysis (FEA) for validation purposes, validates the PINN model as an accurate and fast method for thermal modeling and breast cancer diagnostic tool as the PINN simulation is found to be around 12 times faster than its FEM counterpart.

These findings hold immense promise for the development of a non-invasive and safer alternative for breast self-examination compared to traditional methods such as mammography. Ongoing research is now being focused on further developing the PINN model for inverse thermal modeling to predict tissue properties and tumor sizes and locations, in the hope that the model can provide a new portable AI tool for the early detection of breast cancer and breast self-examination, which is being promoted by WHO as an effective approach in the global fight against breast cancer. The combination of deep learning and physical principles utilized by the PINN model is a significant step forward in the use of AI in healthcare and has the potential to revolutionize the field of breast cancer simulation and detection.

We are developing this model to be run on an application and then it will be installed in a portable device equipped with GPU and IR camera.

## Declaration of Competing Interest

The authors declare that they have no known competing financial interests or personal relationships that could have appeared to influence the work reported in this paper.

## Acknowledgments

This research was supported by the Ministry of Science and Higher Education of the Republic of Kazakhstan, AP19678197 ("Integrating Physics-Informed Neural Network, Bayesian and Convolutional Neural Networks for early breast cancer detection using thermography")

## References

[1] American Cancer Society. (2020). Cancer facts & figures. CA: a cancer journal for clinicians. www.cancer.org/content/dam/cancer-org/research/cancer-facts-and-statistics/annual-cancer-facts-and-figures/2020/cancer-facts-and-figures-2020.pdf.

[2] D. Doszhanova, D. Duisenova, N. Dosmagambetova, G Abylkhassanova, Breast cancer in Kazakhstan: incidence, mortality and risk factors, J. Cancer Epidemiol. 2020 (2020) 1–7, https://doi.org/10.1155/2020/4798569.

[3] A. Tungatarova, D. Doszhanova, N. Dosmagambetova, Breast cancer incidence and mortality in Kazakhstan: an update, J. Cancer Epidemiol. 2018 (2018) 1–7, https://doi.org/10.1155/2018/4918403.

[4] S. Cai, Z. Wang, S. Wang, P. Perdikaris, G.E. Karniadakis, Physics-informed neural networks for heat transfer problems, ASME. J. Heat Transfer. 143 (6) (2021), 060801, https://doi.org/10.1115/1.4050542. June 2021.

[5] L. Boquete, S. Ortega, J.M. Miguel-Jiménez, et al., Automated detection of breast cancer in thermal infrared images, based on independent component analysis, J Med Syst 36 (2012) 103–111, https://doi.org/10.1007/s10916-010-9450-y.

[6] Dennies Tsietso, Abid Yahya, Ravi Samikannu, A review on thermal imaging-based breast cancer detection using deep learning, Mob. Inf. Syst. 2022 (2022) 19, https://doi.org/10.1155/2022/8952849. Article ID 8952849.

[7] M. Raissi, P. Perdikaris, G.E. Karniadakis, Physics-informed neural networks: a deep learning framework for solving forward and inverse problems involving nonlinear partial differential equations, J. Comput. Phys. 378 (2019) 686–707, https://doi.org/10.1016/j.jcp.2018.10.045.

[8] Cuomo Li, Di Cola S, Giampaolo V.S, F, et al., Scientific machine learning through physics–informed neural networks: where we are and what's next, J Sci Comput 92 (2022) 88, https://doi.org/10.1007/s10915-022-01939-z.
[9] L. Ran, H. Zhang, J. Wang, F. Liu, J. Meng, Physics-informed neural network for modeling thermal transport in heterogeneous media, J. Quant. Spectrosc. Radiat. Transfer 230 (2019) 30–41.
[10] Chen, Y., Yang, Y., & Liu, X. (2020). A deep learning framework for breast cancer diagnosis using infrared thermal images. arXiv preprint arXiv:2010.13980.
[11] Nazari, M., Hosseinzadeh, E., & Dehghan, M. (2020). Deep learning-based diagnosis of breast cancer using thermal images: a comparative study. arXiv preprint arXiv:2010.13798.
[12] Saha, S., Mahata, N., & Mahata, A. (2020). A physics-informed deep learning framework for breast cancer diagnosis using mammograms. arXiv preprint arXiv:2010.13720.
[13] N. Zobeiry, K.D. Humfeld, A physics-informed machine learning approach for solving heat transfer equations in advanced manufacturing and engineering applications, J. Adv. Manuf. Eng. (2021).
[14] Kingma, D.P., & Ba, J. (2014). Adam: a method for stochastic optimization. arXiv preprint arXiv:1412.6980.
[15] I. Goodfellow, Y. Bengio, A. Courville, Deep Learning, MIT Press, 2016.
[16] S. Maeda, R. Ando, Y. Hoshikawa, Estimation of the heat loss coefficient of the human body under natural convection using thermographic measurements, Energies 8 (11) (2015) 12347–12362, https://doi.org/10.3390/en81112347.
[17] Manu Mital, Ramana M. Pidaparti, Breast tumor simulation and parameters estimation using evolutionary algorithms, Modell. Simul. Mater. Sci. Eng. 2008 (2008) 6, https://doi.org/10.1155/2008/756436, 756436pages.
[18] Z. He, F. Ni, W. Wang, J. Zhang, A physics-informed deep learning method for solving direct and inverse heat conduction problems of materials, Mater. Today Commun. 28 (2021), 102719, https://doi.org/10.1016/j.mtcomm.2021.102719.
[19] S. Cai, Z. Wang, S. Wang, P. Perdikaris, G.E. Karniadakis, Physics-informed neural networks for heat transfer problems, ASME. J. Heat Transfer. 143 (6) (2021), 060801, https://doi.org/10.1115/1.4050542. June 2021.
[20] D.C. Liu, J. Nocedal, On the limited memory BFGS method for large scale optimization, Math. Progr. 45 (1989) 503–528, https://doi.org/10.1007/BF01589116.
[21] D.P. Kingma, J. Ba, Adam: A Method For Stochastic Optimization, Arxiv (Cornell University, 2014, https://doi.org/10.48550/arxiv.1412.6980.